93-GT-292

THE AMERICAN SOCIETY OF MECHANICAL ENGINEERS
345 E. 47th St., New York, N.Y. 10017

EXPERIMENTAL AND THEORETICAL INVESTIGATIONS OF HEAT TRANSFER IN CLOSED GAS-FILLED ROTATING ANNULI

D. Bohn, E. Deuker, R. Emunds, and V. Gorzelitz
Institute of Steam and Gas Turbines
Technical University of Aachen
Aachen, Germany

ABSTRACT

The prediction of the temperature distribution in a gas turbine rotor containing closed, gas-filled cavities, for example in between two discs, has to account for the heat transfer conditions encountered inside these cavities. In an entirely closed annulus forced convection is not present, but a strong natural convection flow exists, induced by a non-uniform density distribution in the centrifugal force field.

Experimental investigations have been made to analyze the convective heat transfer in closed, gas-filled annuli rotating around their horizontal axis. The experimental set-up is designed to establish a pure centripedal heat flux inside these annular cavities (hot outer, and cold inner cylindrical wall, thermally insulated side walls). The experimental investigations have been carried out for several geometries varying the Rayleigh number in a range usually encountered in cavities of turbine rotors ($10^{07} < Ra < 10^{12}$). The convective heat flux induced for $Ra = 10^{12}$ was found to be a hundred times larger compared to the only conductive heat flux. By inserting radial walls the annulus is divided into 45° sections and the heat transfer increases considerably.

A computer programme to simulate flow and heat transfer in closed rotating cavities has been developed and tested successfully for annuli with isotherm side walls with different temperatures giving an axial heat flux. For the centripedal heat flux configuration, three-dimensional steady state calculations of the sectored annulus were found to be consistent with the experimental results. Nevertheless, analysis of unsteady calculations show that the flow can become unstable. This is analogous to the Bénard problem in the gravitational field.

NOMENCLATURE

a	=	thermal diffusivity
b	=	distance between lateral side walls
c_p	=	specific heat at constant pressure
H	=	distance between outer and inner cylindrical wall
L	=	distance between hot and cold wall ($L = H$ for heat flux directed radially, $L = b$ for heat flux directed axially)
p	=	pressure
$\dot{q}$	=	heat flux from the outer to the inner cylindrical wall
$\dot{q}_\lambda$	=	heat transfer by conduction alone
r	=	radius
R	=	gas constant
T	=	temperature
ΔT	=	temperature difference between hot and cold cylindrical wall
(x,r,φ)	=	axial, radial, circumferential coordinate
(u,v,w)	=	relative velocity components in (x,r,φ) – direction
μ	=	dynamic viscosity
ρ	=	density
ω	=	angular velocity of the cavity
λ	=	thermal conductivity
α	=	section angle

$$Gr = \frac{r_m \cdot \omega^2 \cdot \Delta T \cdot L^3 \cdot \rho^2}{T_m \cdot \mu^2}$$ Grashof number

$$Pr = \frac{\mu \cdot c_p}{\lambda} = \frac{\mu}{\rho \cdot a}$$ Prandtl number

$$Ra = Gr \cdot Pr$$ Rayleigh number

Presented at the International Gas Turbine and Aeroengine Congress and Exposition
Cincinnati, Ohio May 24–27, 1993
This paper has been accepted for publication in the Transactions of the ASME
Discussion of it will be accepted at ASME Headquarters until September 30,1993

$$Re = \frac{\rho \cdot \omega \cdot r_m \cdot L}{\mu}$$ Reynolds number

$$Nu = \frac{\dot{q}}{\dot{q}_\lambda}$$ Nusselt number

$$Ec = \frac{(\omega \cdot r_m)^2}{2 \cdot c_p \cdot \Delta T}$$ Eckert number

Subscripts:

c	=	cold
h	=	hot
i	=	inner
o	=	outer
m	=	arithmetical mean
max	=	maximum
min	=	minimum
SB	=	solid body
w	=	water
0	=	reference
red	=	reduced

Superscripts:

n	=	time level
v	=	iteration level

INTRODUCTION

The development of gas turbines towards higher gas temperatures at the turbine inlet with a simultaneous increase of compressor pressure ratio is a promising trend to increase their thermal efficiency. In connection with this trend attention is being paid to the mechanically and thermally stressed parts of the gas turbine. To estimate these stresses a proper evaluation of temperature distributions in units and components operating in the hottest zones is required. In such a zone temperature nonuniformities may lead to considerable supplementary stresses, the permissible value of which is also determined by the temperature level.

At present only an approximate estimation of the temperature distribution in a gas turbine rotor containing gas-filled enclosures (Fig. 1) is possible. In those cavities a strong, free convective flow is induced. This convection is caused by the buoyancy force corresponding to centrifugal acceleration and temperature differences of the cavity walls. Such a flow increases the heat transfer throughout the cavities considerably.

In the past many theoretical and experimental investigations have been carried out to study the heat transfer in rotating enclosures with a throughflow of cooling fluid, e.g. Ong et al. (1991), Farthing et al. (1992), Owen et al. (1985). For sealed cavities with a purely free convection flow the known theoretical and experimental investigations pertain mainly to constant temperature walls, and are limited to qualitative descriptions of the convective processes. These investigations differ with respect to the direction of the heat flux in the cavity (Fig. 2).

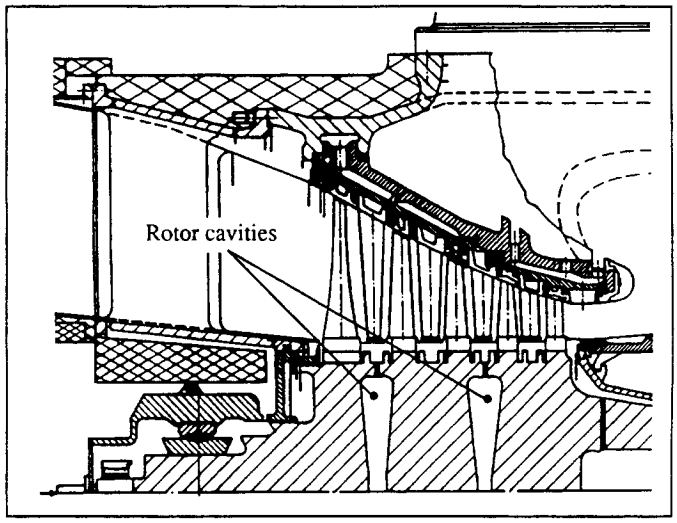

Figure 1: Rotating enclosure in a turbine rotor

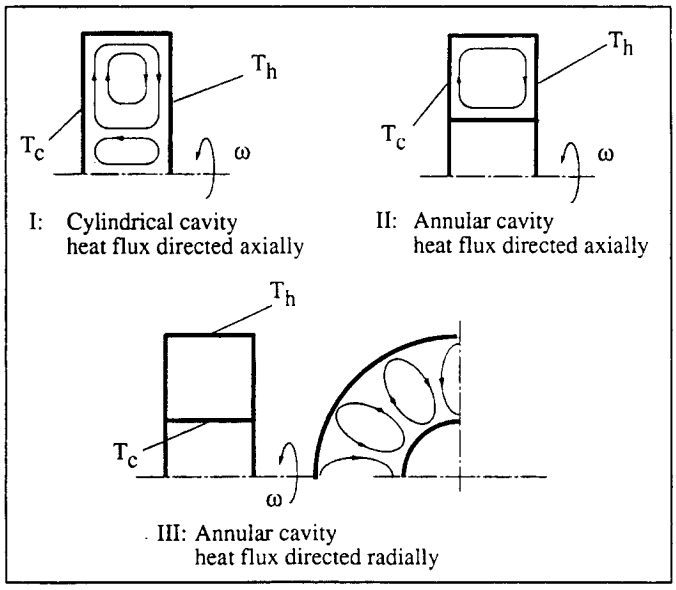

Figure 2: Configurations of rotating enclosures

Most of the investigations have been done for an axially directed heat flux applied on a cylindrical rotating enclosure shown in Fig. 2(I). Kapinos et al. (1981) have performed experimental investigations on heat transfer in an enclosure as described above. They pointed out the influence of Coriolis forces on the fluid motion and compared their experimental results with numerical investigations given by Harada and Ozaki (1975). Abell and Hudson (1975) conducted experiments on an oil-filled rotating cylinder. They deduced a correlation between the Nusselt number and the temperature difference between the hot and cold wall of the cylindrical cavity and the rotational Reynolds number. Chew (1985) also did numerical investigations on heat transfer in these enclosures, producing computations consistent with the experimental results achieved by Abell and Hudson (1975).

Investigations on rotating annular cavities, as in Fig. 2(II), have been conducted by only a few authors. Most of these studies are not even

performed under conditions as encountered in turbo machinery. Müller and Burch (1985) obtained measurements of the transient natural convection in an axially heated rotating annular enclosure simulating geophysical conditions. Similar experimental studies are made by Hignett, Ibbetson and Killworth (1981).

Considering the heat transfer in a cavity such as that shown in Fig. 2(III), Lin and Preckshot (1979) calculated the temperature, velocity and streamline distribution. Zysina-Molozhen and Salov (1977) analyzed experimentally the influence of rotational speed and various thermal boundary conditions on heat transfer in a rotating annular enclosure. The heat flux applied on the test rig was directed centripedally and photographs were taken, showing the flow pattern inside the enclosure. They note the absence of any regular fluid circulation contours in the cavity.

However, there is still a lack of knowledge on rotating sealed cavities, bounded by an outer and an inner cylindrical wall and operating under conditions valid for gas turbines.

At the Institute of Steam and Gas Turbines at the Technical University Aachen experimental and theoretical investigations have been carried out studying the influence of heat flux direction and geometry on the convective heat transfer inside such enclosures. The development of a computer code to simulate free convection flow in rotating annuli is described in a previous paper (Bohn, Dibelius, Deuker and Emunds, 1992), and results are presented for the axial heat flux situation as given in Fig. 2(II).

In this paper experimental and numerical results of convective heat transfer in a rotating closed annulus with radial heat flux (Fig. 2(III)) are presented for conditions very close to turbo machinery operation.

Analyzing the basic conservation equations of mass, momentum and energy (see below) it can be demonstrated that

$$Nu = f(Ra, Re, Pr, H/r_m, b/r_m) \quad (1)$$

The Nusselt number (Nu) is defined as the ratio of the heat flux throughout the cavity to that flux which would occur in solid-body rotation without any motion relative to a co-rotating frame of reference; Nu is thus equal to one for no convection and is greater than one when convection takes place. The rotational Reynolds number (Re) has its origin in the Coriolis force terms in the momentum equations. The rotational Rayleigh number (Ra) is the product of the Grashof number and the Prantl number and is related to the buoyancy term in the radial momentum equation. The Prandtl number is a combination of fluid properties and does not change significantly due to temperature variations.

EXPERIMENTS

Apparatus

The experimental investigations of heat transfer in sealed rotating cavities were performed on three different geometric configurations A, B and C. The test fluid contained in the enclosures is air. The dimensions of the enclosures are given in Fig. 3.

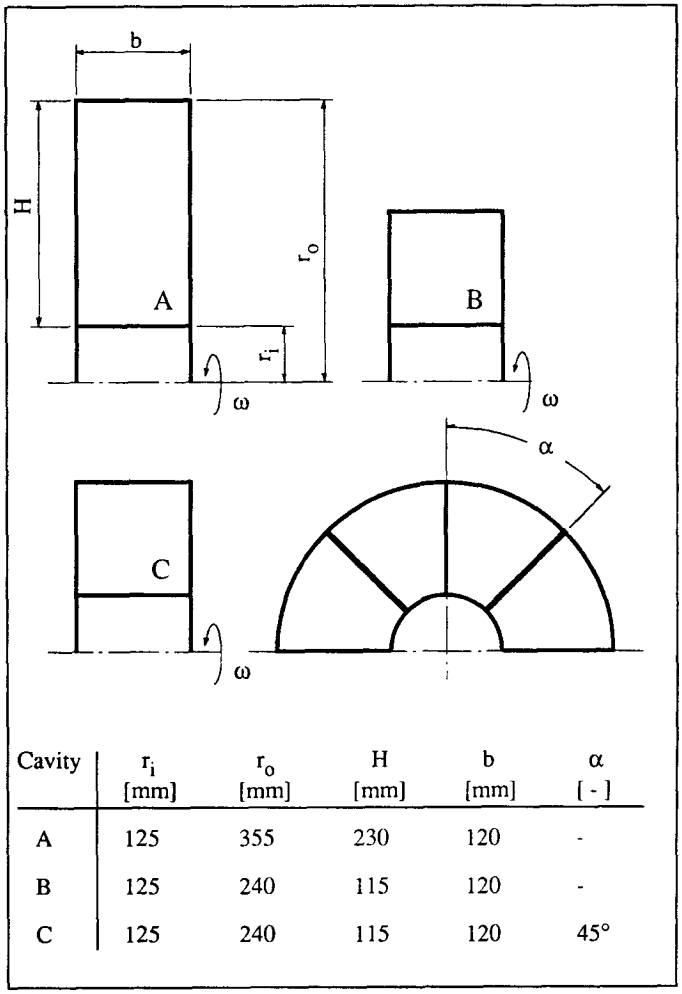

Cavity	r_i [mm]	r_o [mm]	H [mm]	b [mm]	α [-]
A	125	355	230	120	-
B	125	240	115	120	-
C	125	240	115	120	45°

Figure 3: Dimensions of the annular cavities

Test configurations A and B are closed annuli rotating around their horizontal axis. The radius of the inner cylindrical wall as well as the width of the annular cavity are the same for both configuration A and B. Only the radius of the outer cylindrical wall differs for these geometries. The geometrical dimensions of the test cavity C are identical to B, but 8 radial walls divide the annulus into 45° segments. The separation walls do affect the development of the flow in circumferential direction inside the enclosure. This is to study the influence of Coriolis forces on heat transfer.

The experimental investigations on all three configurations were performed at the test rig shown in Fig. 4. This cross-section of the experimental apparatus shows the annular cavity of configuration A. The annulus is formed by two rotor discs with a cylindrical ring on the upper radius between them. The rotor shaft forms the inner cylindrical wall of the annulus. Heat input into the cavity is accomplished by an electrical heater placed at the outer radius of the annulus. To enable a homogenous temperature distribution at the heater surface, the heater is made of a copper ring with a heating wire embedded into a helical groove. Power supply for the electrical heater is realized by a slipping brush assembly. Heat is removed out of the

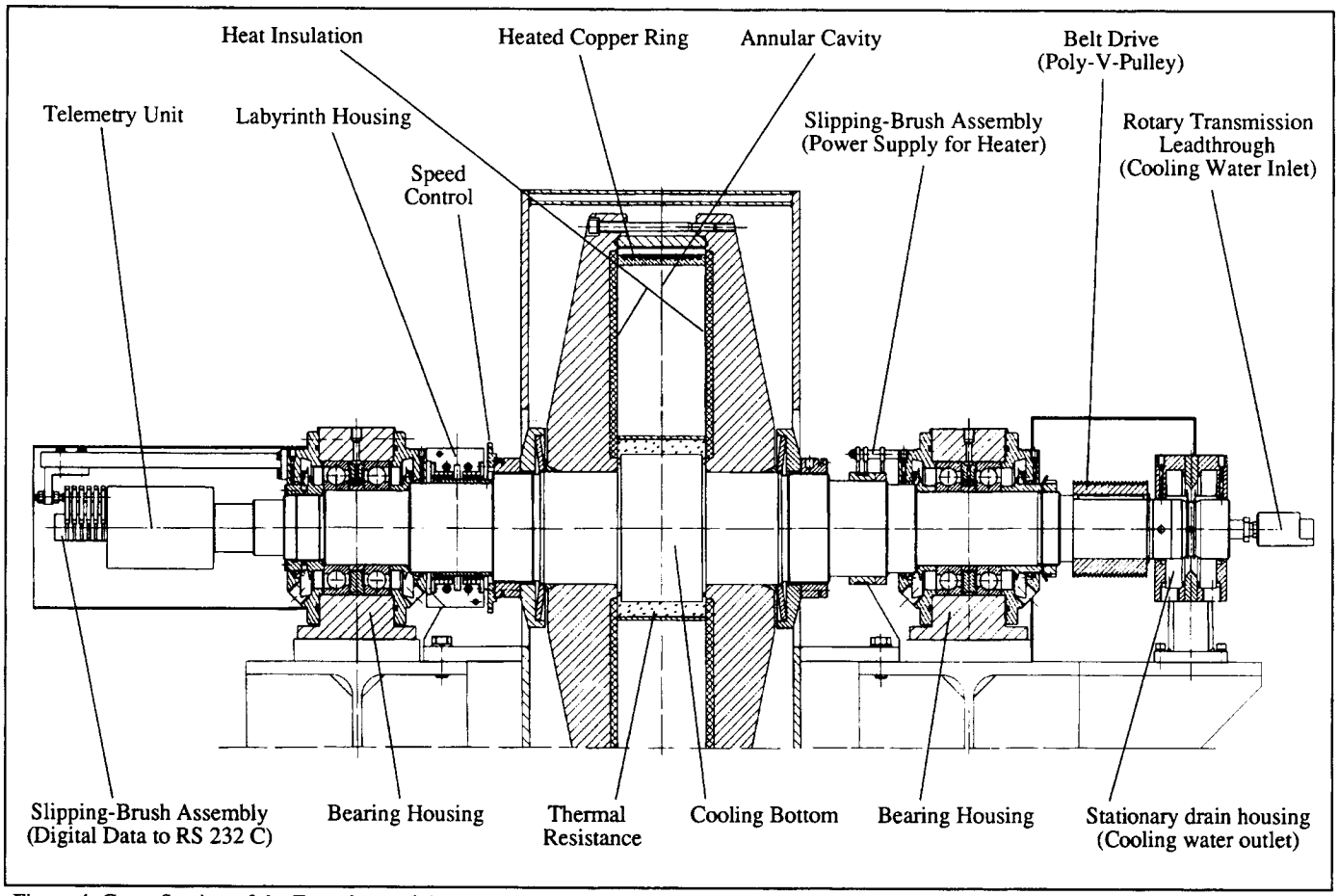

Figure 4: Cross Section of the Experimental Apparatus

cavity by the water-cooled rotor shaft. The water enters the rotor shaft by a rotary transmission leadthrough, flows to the cooling bottom, and, concentric to the inflow, back out to a drain housing. Both lateral surfaces of the annulus are thermally insulated. The heat insulating panels are made of a bounded honeycomb sandwich construction. The honeycomb consists of an aramid-fibre paper treated with a heat-resistant phenolic resin. Both bounded face sheets consist of a phenolic resin prepreg. Using this sandwich construction a thermal conductivity of the heat insulating panels is achieved, which is virtually as little as that of air. The cavity can be pressurized while running the rotor by using a labyrinth housing. The rotor shaft is driven by a DC motor using a belt drive. Measurements of the rotational speed are accomplished by mounting a perforated disc on the shaft and using a coil to produce a voltage spike when one of the perforations passes it. Double bearings are installed at the ends of the rotor shaft enabling steady rotation.

Heat fluxes from the outer cylindrical wall to the working fluid and from the working fluid to the inner cylindrical wall are determined by measuring the temperature differences across a thermal resistance (Fig. 5).

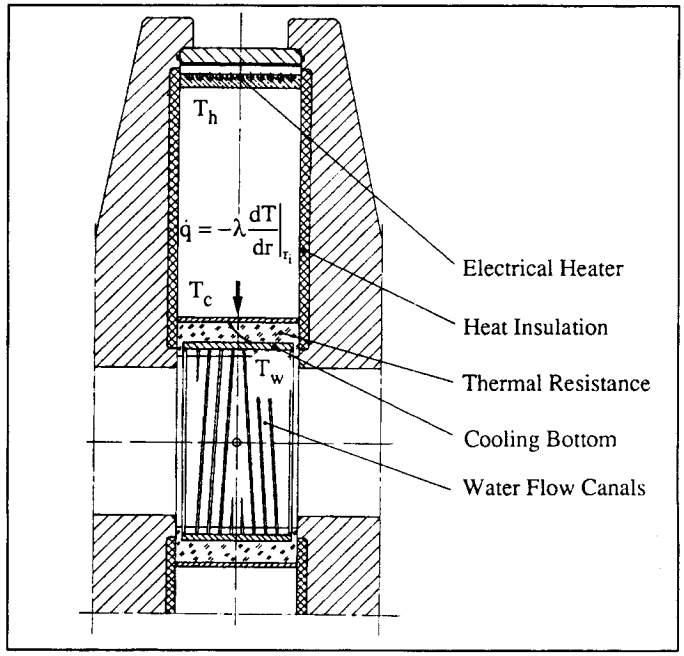

Figure 5: Heat flux measuring device

The thermal resistance consists of an epoxy layer held between the rotor shaft and a steel tube concentric to it. Conductivity and thickness of it are chosen so that a sufficient temperature drop on it can be obtained due to the expected heat fluxes. Temperatures are measured using thin-film resistance thermometers of platinum (5 x 5 x 0.3 mm) installed prior to pouring the epoxy layer. Nine thermometers are located across the length of the thermal resistance on its outer and inner surface. The temperature distribution on the rotor surface, inside as well as outside the enclosure, is recorded by an additional 18 thin-film thermometers. A telemetry unit, fixed on one end of the rotor shaft, registers the analogue signals of the resistance thermometers and converts them into digital. The digital data are transmitted out of the telemetry unit to an interface of a personal computer (RS 232 C) by a slipping-brush assembly. The digital circuit can measure the absolute temperature of a resistance thermometer to an accuracy of 0.01 °C.

The dimensions of cavity configuration B on this experimental apparatus are realized only by mounting a smaller heated cylindrical ring between the two rotor discs. This also gives the basic dimensions of configuration C. In contrast to cavity B, cavity configuration C is not an annulus, but it is divided into 45° segments by 8 heat insulating panels (thickness of 10 mm).

Procedure

During the experiments the rotor speed, the cavity pressure, electric current to the heater, and the mass flow rate of cooling water were kept at constant levels. The maximum rotor speed is set up to 3500 rev/min. The maximum cavity pressure is set up to 4 bar. The maximum temperature at the outer heated cylindrical wall is varied up to 100 °C. The minimum temperature at the cooling bottom is fixed by the cooling water which is taken from a water tap (about 15 °C in summer and 8 °C in winter).

Experimental test loops are continued until thermal conditions reach a steady state. Data from all measuring points are recorded repeatedly at intervals of two minutes. To meet the criterion of steady state conditions the relative rate of temperature changes should not exceed 1% for temperatures of about 10 °C and 0.1% for temperatures of about 100 °C during an observation period of ten minutes. The heat flux throughout the cavities is calculated from the measured temperature drop across the epoxy layer of known thermal conductivity.

Experimental results

The governing equations (eqns. 4 to 8, see below) make clear that the Nusselt number depends mainly on three dimensionless parameters, i. e. the Prandtl number, the rotational Rayleigh number Ra, and the rotational Reynolds number Re. The geometry is given by the aspect H/r_m and the ratio b/r_m. (For configuration C the section angle occurs additionally.) In the present study the Prandtl number was not varied. Therefore, no information is obtained from the experiments regarding the dependence on Pr. Consequently, for a given fluid and a specified geometric configuration, i. e. for fixed H/r_m and b/r_m ratio, it might be expected that

$$Nu = f(Ra, Re) \tag{2}$$

Since

$$Ra = (\Delta T/T_m) \cdot (H/r_m) \cdot Re^2 \cdot Pr^2 \tag{3}$$

it is apparent that for a fixed value of $\Delta T/T_m$ the Re number cannot be treated as an independent variable. Due to the permissible temperature levels of the epoxy layer in the experimental set-up, the ratio $\Delta T/T_m$ can only be varied in a small range. Furthermore, it was found that the values of $\Delta T/T_m$ which could be realized in experiment, decrease continuously as the Ra number increases. Therefore, for all three cavity configurations A, B, and C we only consider the Nusselt number's dependence on the rotational Rayleigh number and give a correlation equation for the corresponding Re number.

Values were obtained from the experiments for the temperature distribution at the cavity walls at different heat fluxes, rotational speeds and cavity pressures. The surface temperatures of the heater and the thermal resistance were virtually isothermal. Only in a very narrow region at the lateral ends of the thermal resistance did the temperature differ from the mean surface temperatures, but by no more than 1.5 K and only for very large rotational speeds. However, the local heat flux along the length of the thermal resistance is virtually constant. Average surface temperatures were calculated and used throughout the analysis of the heat transfer results. Although this introduces some error into the results, it is not expected to have a significant influence on the Nusselt number.

The heat loss through the insulating lateral walls was estimated from the temperature drop across the walls of known thermal conductivity. The heat loss decreases with higher rotational speeds due to the friction on the outer rotor surface. For low rotational speeds of about 250 r.p.m. the heat loss is about 20 % of the total heat input. At high rotational speeds of about 3500 r.p.m. this amounts to no more than 10%. In spite of varying rotor speed and cavity pressure at constant Ra and Re numbers the Nu numbers were always reproducable in a max. range of ±1%.

The influence of the radiative heat transfer on the heat flux throughout the cavity was calculated. For Nusselt numbers higher than 30, this amounts to no more than 2 % of the total heat flux and, therefore, has not been taken into account.

In Figures 6, 7, and 8 the Nusselt number is shown as a function of Ra for cavity configuration A, B, and C, respectively. The experimental points meet satisfactorily the straight line which is calculated from the data by means of a least-square fit. The figures show that the heat transfer depends strongly on the Rayleigh number.

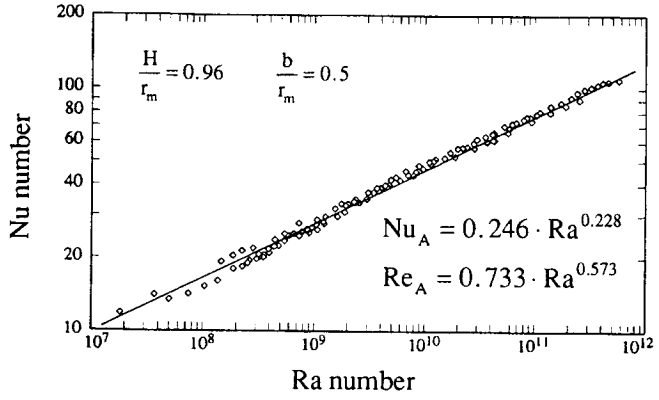

Figure 6: Heat transfer in cavity A, obtained at different rotational speeds, and cavity pressures

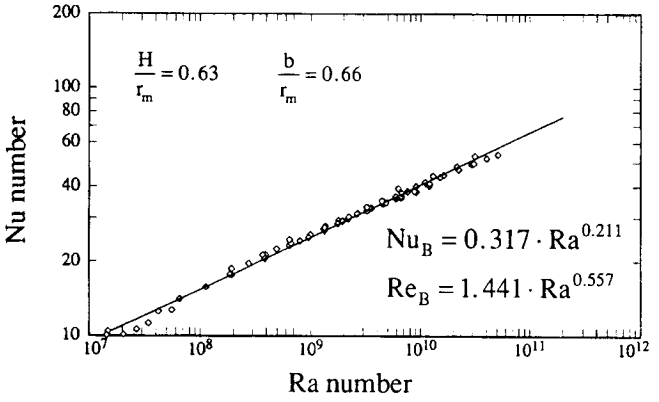

Figure 7: Heat transfer in cavity B, obtained at different rotational speeds, and cavity pressures

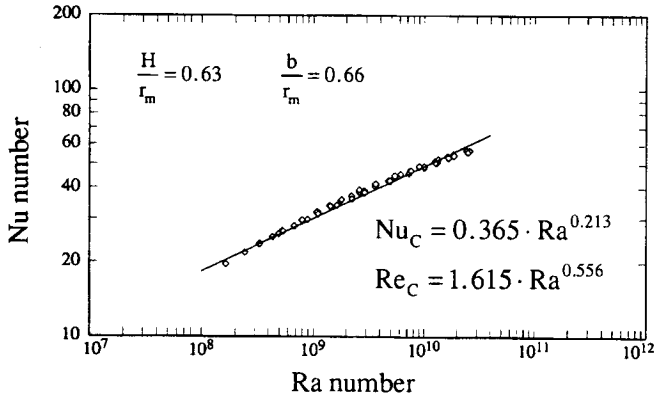

Figure 8: Heat transfer in cavity C, obtained at different rotational speeds, and cavity pressures

In Fig. 9 results for configurations A and B are compared. With the reduction of the outer radius the distance L between hot and cold wall is reduced, which is a very sensitive parameter for natural convection flows. Note that Ra ~ L^3 and Re ~ L . But the ratio H/r_m and the ratio b/r_m are also changed by the reduction of the outer radius. Thus, without further information it is not possible to separate the influences of the parameters mentioned above on the Nu number. However, it is noteworthy that the Nu number does not change very much due to this geometric variation. Note that for the same Ra numbers the Re number in case B is nearly twice as that in case A.

A numerical study has been performed to show the influence of aspect ratio b/r_m on the heat transfer. Increasing b by a factor of 2 decreases the Nu number by about 4.7 %, and, when increased by a factor of 3, Nu was found to be 7.6 % smaller. Although these calculations have been done for configuration C at Ra = 10^9, similar results may be expected for cases A and B. Therefore, it is believed, that the b/r_m ratio (which changes only by 34% from case A to case B) has only a weak influence on the Nu number.

In Fig. 10 configurations B and C are compared. The only difference between the two geometries is the insertion of radial seperation walls in case C, but this does not affect the other dimensionless parameters given in eqn. (1).

The insertion of separation walls attenuates the relative circumferential velocity inside the cavity, resulting in a decrease of the radial component of the Coriolis force (see eqn. 6). In the previous paper (Bohn et al., 1992) it was pointed out that Coriolis forces have a dampening effect on the flow. Thus, attenuating the Coriolis forces by inserting separation walls the natural convection flow inside the cavity is strengthened so that the heat transfer increases. This is confirmed by the results shown in Fig. 10.

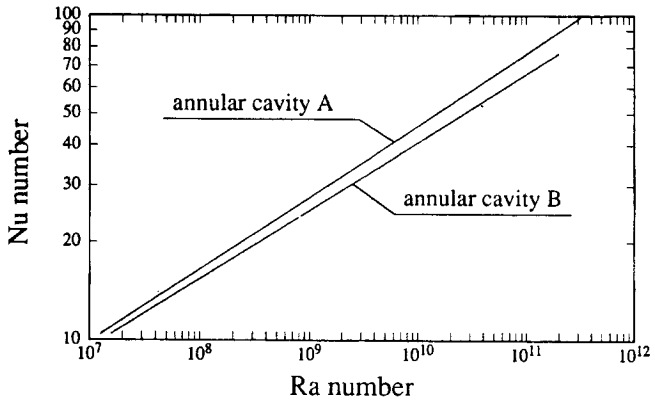

Figure 9: Comparison of cavity configurations A with B

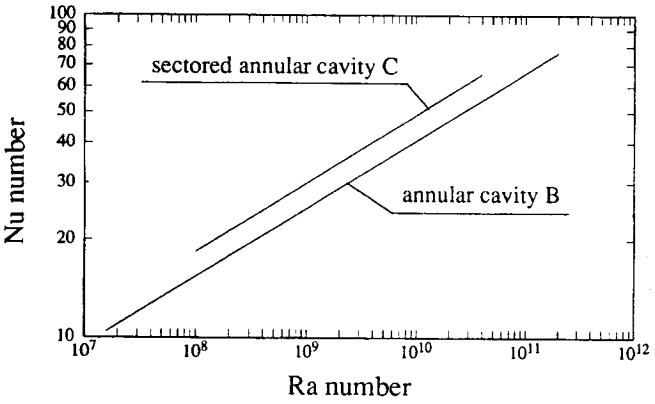

Figure 10: Comparison of cavity configurations B with C

NUMERICAL INVESTIGATION

Though the geometry of the cavities under consideration is quite simple, the flow is characterized by a complex interaction of convection, viscous forces, pressure forces, buoyancy effects and Coriolis forces. In the previous paper (Bohn et al., 1992) flow structure and heat transfer have been analyzed for the axial heat flux situation, and special attention has been given to the buoyancy and Coriolis forces, which were found to be the most important terms to determine the heat transfer.

In the present case of a pure centripedal heat flux an additional difficulty occurs: the temperature gradient is in opposite direction to the centrifugal force, and the flow is basically unstable.

A similar, well known situation is found in the gravitational field: a fluid layer between two horizontal plates, where the temperature at the bottom surface is greater than the temperature at the top wall. In that case the temperature gradient is in opposite direction to the gravitational force, and an unstable flow called Bénard convection occurs. It is known from literature that in this case the flow pattern also depends on the thermal boundary conditions of the side walls and the initial conditions (see, for example, Liang et al., 1969).

From our experiments, no information about the flow structure and only little information about the thermal conditions at the side walls can be obtained. Therefore, for the time being we restrict our numerical analysis to the idealized case of adiabatic side walls and isothermal cylindrical walls. Though this is not a detailed investigation of the flow pattern inside our test cavity, it may highlight some basic features of this type of flow and can be considered as a basic case that is independent of special thermal conditions at the side walls.

Basic Modelling Assumptions

The radial heat flux was modelled assuming the temperatures at the cylindrical walls were different but uniformly distributed, while all other walls (the two side walls and the separation walls in radial direction) were assumed to be adiabatic.

The computer programme solves the conservation equations for mass, momentum and energy. All computations were carried out for air, the density is calculated by the ideal gas law, and all other properties are treated as functions of temperature. Some common assumptions for natural convection flows are made: in the viscous terms of the momentum equations the compressiblility is neglected because the velocities at this type of flow are very small. In the energy equation the influence of the dissipation and pressure changes are assumed to be negligible too, due to very small Eckert numbers (Ec < 0.1). The flow is assumed to be laminar in the range of Gr numbers considered. The previously presented results verify this assumption for the axial heat flux situation, see D. Bohn et al. (1992) for a more detailed discussion.

The Governing Equations

The steady state governing equations are derived and declared comprehensively by D. Bohn et al. (1992). Now, the code has been extended to simulate unsteady flow. The dimensionless form of the equations reads:

$$\frac{\partial\bar{\rho}}{\partial\bar{t}}+\frac{1}{\bar{r}}\cdot\left(\frac{\partial\bar{\rho}\bar{u}\bar{r}}{\partial\bar{x}}+\frac{\partial\bar{\rho}\bar{v}\bar{r}}{\partial\bar{r}}+\frac{\partial\bar{\rho}\bar{w}}{\partial\varphi}\right)=0 \tag{4}$$

$$\frac{\partial\bar{\rho}\bar{u}}{\partial\bar{t}}+\frac{1}{\bar{r}}\left(\frac{\partial}{\partial\bar{x}}\bar{\rho}\bar{r}\bar{u}\bar{u}+\frac{\partial}{\partial\bar{r}}\bar{\rho}\bar{r}\bar{v}\bar{u}+\frac{\partial}{\partial\varphi}\bar{\rho}\bar{w}\bar{u}\right)- \tag{5}$$

$$-\frac{Pr}{\bar{r}}\cdot\left(\frac{\partial}{\partial\bar{x}}\left(\bar{\mu}\bar{r}\frac{\partial\bar{u}}{\partial\bar{x}}\right)+\frac{\partial}{d\bar{r}}\left(\bar{\mu}\bar{r}\frac{\partial\bar{u}}{\partial\bar{r}}\right)+\frac{\partial}{\partial\varphi}\left(\frac{\bar{\mu}}{\bar{r}}\frac{\partial\bar{u}}{\partial\varphi}\right)\right)=-\frac{\partial\bar{p}_{red}}{\partial\bar{x}}$$

$$\frac{\partial\bar{\rho}\bar{v}}{\partial\bar{t}}+\frac{1}{\bar{r}}\left(\frac{\partial}{\partial\bar{x}}\bar{\rho}\bar{r}\bar{u}\bar{v}+\frac{\partial}{\partial\bar{r}}\bar{\rho}\bar{r}\bar{v}\bar{v}+\frac{\partial}{\partial\varphi}\bar{\rho}\bar{w}\bar{v}\right)- \tag{6}$$

$$-Pr\cdot\left(\frac{\partial}{\partial\bar{x}}\left(\bar{\mu}\bar{r}\frac{\partial\bar{v}}{\partial\bar{x}}\right)+\frac{\partial}{\partial\bar{r}}\left(\bar{\mu}\bar{r}\frac{\partial\bar{v}}{\partial\bar{r}}\right)+\frac{\partial}{\partial\varphi}\left(\frac{\bar{\mu}}{\bar{r}}\frac{\partial\bar{v}}{\partial\varphi}\right)\right)=-\frac{\partial\bar{p}_{red}}{\partial\bar{r}}-$$

$$-Pr\frac{\bar{\mu}}{\bar{r}^2}\left(\bar{v}+2\frac{\partial\bar{w}}{\partial\varphi}\right)-\bar{\rho}\frac{\bar{w}^2}{\bar{r}}+2\bar{\rho}\bar{w}\frac{L}{r_m}Re\cdot Pr-\bar{\rho}_{SB}\bar{r}\frac{T_m}{T}\frac{L}{r_m}Ra\cdot Pr\cdot\bar{T}$$

$$\frac{\partial\bar{\rho}\bar{w}}{\partial\bar{t}}+\frac{1}{\bar{r}}\left(\frac{\partial}{\partial\bar{x}}\bar{\rho}\bar{r}\bar{u}\bar{w}+\frac{\partial}{\partial\bar{r}}\bar{\rho}\bar{r}\bar{v}\bar{w}+\frac{\partial}{\partial\varphi}\bar{\rho}\bar{w}\bar{w}\right) \tag{7}$$

$$-Pr\left(\frac{\partial}{\partial\bar{x}}\left(\bar{\mu}\bar{r}\frac{\partial\bar{w}}{\partial\bar{x}}\right)+\frac{\partial}{\partial\varphi}\left(\frac{\bar{\mu}}{\bar{r}}\frac{\partial\bar{w}}{\partial\varphi}\right)+\frac{\partial}{\partial\bar{r}}\left(\bar{\mu}\bar{r}\frac{\partial\bar{w}}{\partial\bar{r}}\right)\right)=-\frac{1}{\bar{r}}\frac{\partial\bar{p}_{red}}{\partial\varphi}-$$

$$-Pr\frac{\bar{\mu}}{\bar{r}^2}\left(\bar{w}-2\frac{\partial\bar{v}}{\partial\varphi}\right)-\bar{\rho}\frac{\bar{v}\bar{w}}{\bar{r}}-2\bar{\rho}\bar{v}\frac{L}{r_m}\cdot Re\cdot Pr$$

$$\frac{\partial\bar{\rho}\bar{T}}{\partial\bar{t}}+\frac{1}{\bar{r}}\frac{\partial}{\partial\bar{x}}\left(\bar{\rho}\bar{r}\bar{u}\bar{T}-\frac{\bar{\lambda}\bar{r}}{\bar{c}_P}\frac{\partial\bar{T}}{\partial\bar{x}}\right)+\frac{1}{\bar{r}}\frac{\partial}{\partial\bar{r}}\left(\bar{\rho}\bar{r}\bar{v}\bar{T}-\frac{\bar{\lambda}\bar{r}}{\bar{c}_P}\frac{\partial\bar{T}}{\partial\bar{r}}\right)+ \tag{8}$$

$$+\frac{1}{\bar{r}}\frac{\partial}{\partial\varphi}\left(\bar{\rho}\bar{w}\bar{T}-\frac{\bar{\lambda}}{\bar{r}\bar{c}_P}\frac{\partial\bar{T}}{\partial\varphi}\right)=0$$

Herein the Re number occurs within the Coriolis terms, while the Ra number is related to the buoyancy term. The dimensionless variables marked with an overbar result from the following definitions:

$$u=\bar{u}\cdot\frac{a_0}{L};\qquad p=\bar{p}\cdot\frac{\rho_0\cdot a_0^2}{L^2};\quad \rho=\bar{\rho}\cdot\rho_0;$$

$$T=\bar{T}\cdot\Delta T+T_m;\quad \lambda=\bar{\lambda}\cdot\lambda_0;\qquad \mu=\bar{\mu}\cdot\mu_0;$$

$$c_p=\bar{c}_p\cdot c_{p0};\quad x=\bar{x}\cdot L;\qquad r=\bar{r}\cdot L;\qquad t=\bar{t}\cdot\frac{L^2}{a_0}$$

The fluid properties λ_0, a_0, ρ_0, μ_0, c_{p0} are evaluated for T_m as the reference temperature ($T_m = 0.5\ (T_h+T_c)$, see Fig. 2(III)). They have also been used to calculate the values of Re, Ra, and Pr. To obtain the reduced pressure defined by

$$p_{red} = p - p_{SB}$$

the radial momentum equation for a rotating solid body at constant temperature is used:

$$-\frac{\partial p_{SB}}{\partial r} + \rho_{SB} \cdot \omega^2 \cdot r = 0$$

$$\rho_{SB} = \frac{p_{SB}}{R \cdot T_m}$$

The Numerical Procedure

The system of coupled differential equations is solved numerically with a finite volume scheme. A non-uniform staggered grid is defined, with T and p being calculated at the main grid points and u,v,w being calculated at locations which are midway between the main grid points. In the employed "hybrid" differencing method upwind differencing is used for the convective terms when the cell-Peclet-number is greater than 2, otherwise central differencing is used for these terms.

The unsteady pressure correction is based on an iteration procedure defined by Patankar and Spalding (1972). From the momentum equations (not considering the source terms) for the time step n (eqn. 9) and for the actual time iteration (Index ν , eqn. 10)

$$\frac{\rho \cdot \vec{v}^n - \rho \cdot \vec{v}^{n-1}}{\Delta t} = -\nabla p^n - \left(\vec{v}^n \cdot \nabla\right)\rho \cdot \vec{v}^n + \mu \cdot \nabla^2 \vec{v}^n \qquad (9)$$

$$\frac{\rho \cdot \vec{v}^* - \rho \cdot \vec{v}^{n-1}}{\Delta t} = -\nabla p^\nu - \left(\vec{v}^* \cdot \nabla\right)\rho \cdot \vec{v}^* + \mu \cdot \nabla^2 \vec{v}^* \qquad (10)$$

an equation for the unsteady pressure correction p' can be derived (by neglecting the convective and diffusive terms),

$$\nabla^2 p' = \frac{1}{\Delta t}\left(\nabla \cdot \rho \vec{v}^*\right) \qquad \text{with} \quad p^\nu = p' + p^{\nu-1} \qquad (11)$$

where the continuity equation is used. Equation (11) has to be solved for the the velocity field $\vec{v}^*$ resulting from equation (10). The iteration process has to be continued until p' is sufficiently small. At this time the velocity field $\vec{v}^*$ is the correct velocity field for the new time level $\vec{v}^n$ and the pressure p^ν is the correct pressure p^n.

Theoretical Results For The Closed Rotating Sectored Cavity (Steady State Calculations)

In the first instance we restricted ourselves to the sectored geometry (Configuration C) because the number of grid points required in circumferential direction is considerably smaller in that case. The calculations were carried out on a numerical grid containing about 36000 grid points. Because the experiments gave steady state results we started the numerical simulation with a steady algorithm keeping in mind that the flow might be unsteady. A more detailed discussion of the unsteady behaviour of the flow is given below.

Figure 11 shows a comparison of the Nu numbers taken from experiment and from numerical (steady) simulation for a wide range of Ra numbers. Over the entire range the numerically-calculated Nu numbers are slightly greater than those achieved by experiment. One reason for this deviation is the boundary condition of the side walls which were treated as adiabatic for the numerical simulation. By adding the heat losses of the side walls to the heat transferred throughout the thermal resistance at the inner radius of the cavity the Nu numbers obtained from experiment increase by about 10 to 20%. Thus, the difference between experiment and numerical calculation becomes much smaller and the steady numerical algorithm was found to be a sufficient predictor of the heat transfer.

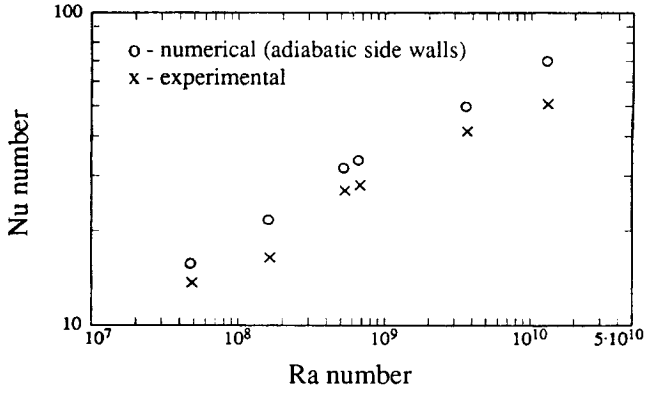

Figure 11: Comparison of the Nu number obtained from experiment and from numerical simulation for various Ra numbers

As a typical example, Figure 12 shows the flow field in radial and circumferential direction for three axial positions and the temperature distribution for the medium axial position. The calculation was carried out for air at T_m=330,3 K which gives a Prandtl number of 0,70. In all three axial positions the fluid circulates in boundary layers, and nearly no motion occurs in the core region. The flow pattern does not change significantly in axial direction.

In Table 1 the maxima and minima of the velocity components at the medium axial position are compared. The axial velocity component is significantly smaller than the radial and circumferential component. At other axial positions the results are similar. This makes clear that the mean flow takes place in the r - φ plane.

direction	max. size [m/s]	min. size [m/s]
axial	0,11	-0,071
radial	0,893	-0,821
circum-ferential	0,78	-0,70

Table 1: Comparison of the maxima and minima of the velocity components at medium axial position in the cavity ($Ra = 4.86 \cdot 10^7$, $Re = 3.00 \cdot 10^4$)

a) Flow field in the r - φ - plane at x / b = 0.001

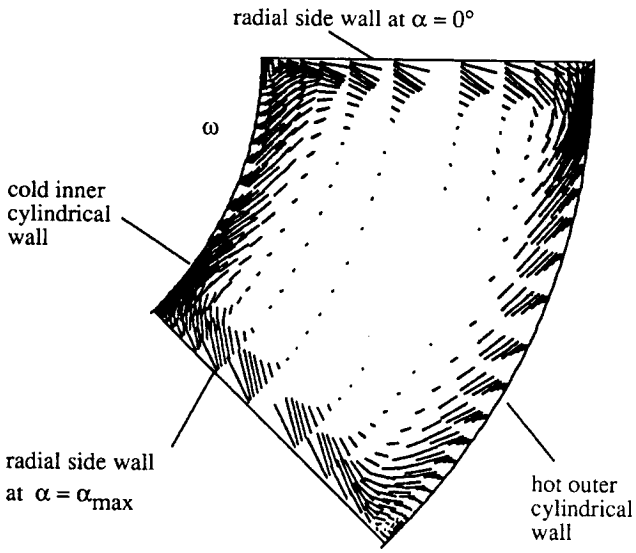

b) Flow field in the r - φ - plane at x / b = 0.5

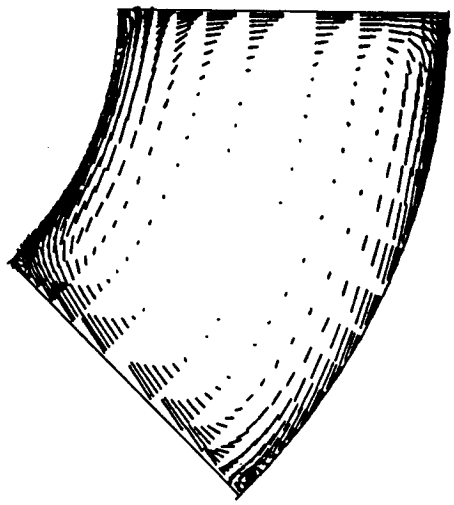

c) Flow field in the r - φ - plane at x / b = 0.999

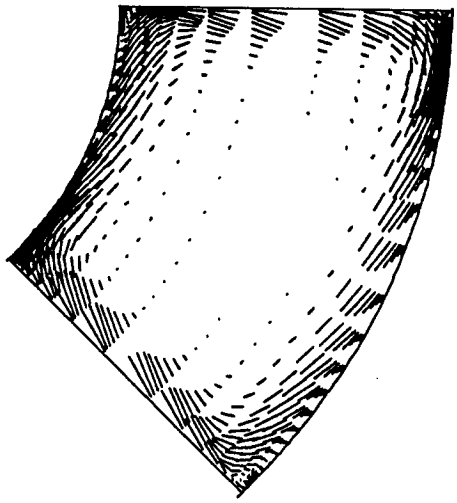

d) Temperature distribution (x / b = 0.5)

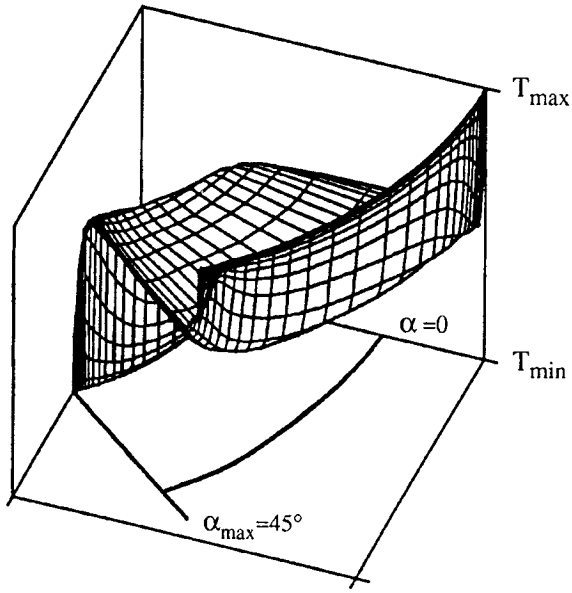

Figure 12: Flow pattern at x/b = (0.001, 0.5, 0.999), temperature distribution at x/b = 0.5 in a rotating cavity ($Ra = 4.86 \cdot 10^7$, $Re = 3.00 \cdot 10^4$)

The direction of rotation of the flow can be explained with the Coriolis- and buoyancy terms in the radial momentum equation (eqn.6). An estimation of the order of magnitude shows that the buoyancy term and the Coriolis term are much greater than the convective and diffusive terms ($\bar{v} << \omega r_m$ and $\mu/\rho << \omega r_m^2$, respectively). At the hot wall $\overline{T}$ is greater than zero giving a negative buoyancy term. Therefore, the Coriolis term must be positive to balance the buoyancy term, which effects a positive circumferential velocity component at the hot wall. At the cold wall the buoyancy term is positive and, therefore, the Coriolis term and the velocity component in circumferential direction has to be negative.

Moving from the cold wall to the hot wall along the radial separation wall at $\alpha = 0$, the fluid has a nearly constant temperature $T \approx 0.5 (T_{max} + T_{min})$ (Fig. 12d). A large positive temperature gradient occurs when the fluid reaches the hot wall. Similarly, near the cold wall at $\alpha = \alpha_{max}$ a large negative temperature gradient occurs. In the core itself a nearly constant temperature is found, where heat is neither conducted in radial direction nor in circumferential direction. Thus, the heat transfer is strictly determined by convection in the boundary layers.

In Figure 13 the distribution of the local Nu number at the hot outer and the cold inner cylindrical wall of the rotating annulus is plotted for a medium axial position. At the outer cylindrical wall most of the heat is transferred in the region where the cold fluid reaches this wall (great temperature gradients occur, see Fig. 12d). Moving along the hot wall the fluid is warmed up. Therefore, the heat transfer (represented by the local Nu number) decreases. Due to the edge vortex in the corner of the hot wall and the radial wall at $\alpha = \alpha_{max}$ (see Fig. 12a,b,c) fluid with a lower temperature is transported back to the hot wall. This effect leads to an increase of the local Nu number in this region. Similarly, at the cold inner cylindrical wall an analogous effect is found at $\alpha = 0$.

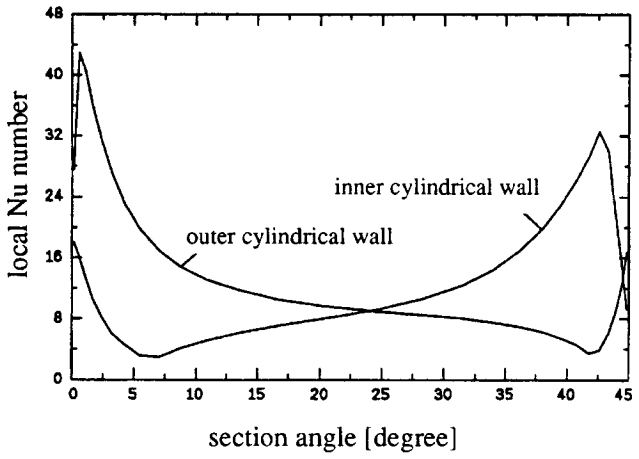

Figure 13: Heat transfer at the hot and the cold cylindrical wall at a medium axial position
($Ra = 4.86 \cdot 10^7$, $Re = 3.00 \cdot 10^4$)

Results of unsteady calculations for a rotating closed cavity

To identify some more basic features of this type of flow, unsteady calculations have been carried out for a special test geometry ($H/b = 1$, $r_m/b = 3$, section angle $\alpha = 45$ degree). This geometry is quite favourable for the comparison of the axial and the radial heat flux situation because the characteristic length for the buoyancy effects, i.e. the distance L between the hot and the cold wall, is the same in both cases. Thus, the Re number and the Ra number are the same for the two kinds of heat fluxes. Calculations were carried out for an axial and a radial heat flux (for $T_m = 575$ K, $Ra = 8 \cdot 10^5$, $Re = 6 \cdot 10^4$). Both calculations were started at $t = 0$ with a relative velocity field equal to zero and heat conduction as an initial condition for temperature field.

To ensure time accuracy, the time step Δt was set very small. A CFL number defined by

$$CFL = \frac{u \cdot \Delta t}{\Delta x}$$

u = maximum relative velocity in the flow field

Δx = minimum distance of two grid points

may be used to characterize the unsteady conditions. This number was smaller than one for the unsteady calculations. The calculation of the radial heat flux configuration shown in Fig. 14 took more than 10 000 time steps.

In Figure 14a the Nu number at the hot wall vs. the time is plotted for the unsteady calculation of the axial heat flux configuration and the steady and unsteady simulation of the radial heat flux configuration.

In the axial case it can be seen that the unsteady calculation converges to a steady state rather quickly. In Figure 14b the distribution of the maximum time residuum from the conservation equations for each time step is plotted. In the axial case a strong increase of the residuum occurs at the beginning of the simulation followed by a continuous decrease.

The time-dependent distribution of the Nu number (Fig. 14a) for the radial heat flux configuration is irregular during the whole simulation time of 18 seconds. A more detailed flow simulation was not performed because of drastically-increased CPU time-requirement. The calculation was performed on an IBM 3090 Computer using the vector facilities and required more than 10 CPU hours. Additionally, Figure 14a shows the value of the Nu number calculated with the steady state algorithm. For the unsteady calculation it is not possible at this time to deduce a tendency, i. e. whether the flow will converge to a steady state or become periodical or even remain irregular.

An unsteady behaviour of natural convection flow is well known from the Bénard convection. This type of flow can be approached by the rotating annulus with radial heat flux direction by setting a very large r_m/H ratio. The angular velocity ω must fit the condition that the centrifugal acceleration $\omega^2 r_m$ equals the gravity acceleration. The Coriolis forces are neglegible for this extreme situation.

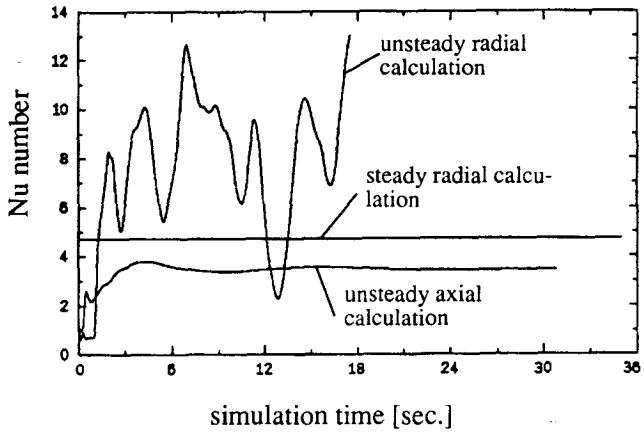

Figure 14a: Development of Nu number for the axial and the radial heat flux configuration

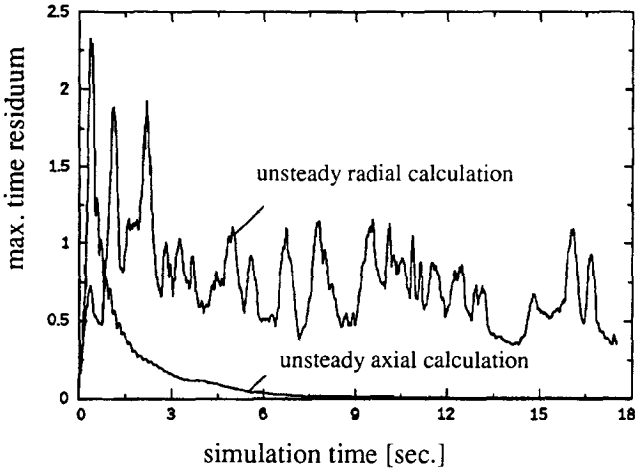

Figure 14b: Distribution of the maximal time residuum for the axial and the radial heat flux configuration

It is reported by many authors that the flow pattern of Bénard convection changes significantly several times with increasing Ra number. For Ra < 1700 no fluid motion at all is observed. At Ra numbers of about 10^4 a steady two-dimensional flow is established. With further increases of the Ra number the flow becomes periodically unsteady, then irregularly unsteady (thermals rising from the bottom and the top surface) and at least fully turbulent. (See D. J. Tritton (1988) for details and further references.)

SUMMARY AND CONCLUSIONS

Investigations have been carried out on convective heat transfer in closed annuli rotating around their horizontal axis. A pure centripedal heat flux throughout the cavities was applied by heating the outer and cooling the inner cylindrical wall. Both lateral walls of the annular cavities were thermally insulated.

Measurements have been performed varying the Rayleigh number in a range usually encountered in the gas-filled cavities of gas turbine rotors (10^{07} < Ra < 10^{12}). Varying the ratio from H/r_m= 0.96 to H/r_m= 0.63 yields no significant influence on the Nu number. With the annulus divided into sections, by inserting radial separation walls, the influence of the Coriolis forces is reduced resulting in an increase of heat transfer.

Theoretical investigations for the basic case of isothermal cylindrical walls and adiabatic side walls have been made for the sectored annular cavity. The calculations were carried out using a steady state numerical algorithm. The results obtained for the convective heat transfer are consistent with the experiments.

In addition, unsteady calculations have been carried out for an axial and centripedal heat flux applied on the rotating annulus. For the axial heat flux steady state conditions were reached rather quickly. For the centripedal heat flux, within 10 hours CPU time, no prediction can be made whether the flow will become periodic, steady, or remain irregular.

The numerical results show, that the flow inside the cavity may be affected by instability phenomena. From the experiments no information can be obtained about the flow structure. However, the heat losses through the side walls, which were inevitable during the experiments, could serve to stabilize the flow and to establish steady state conditions. On the other hand, Zysina-Molozhen et al., who took photographs from the flow inside a rotating cavity with centripedal heat flux, note the absence of any regular fluid circulation contours.

Further experimental and theoretical investigations should work out the conditions for instability and show the influence of the thermal boundary conditions of the side walls on the flow and the heat transfer in the cavity.

ACKNOWLEDGEMENT

The authors thank the Arbeitsgemeinschaft Hochtemperatur-Gasturbine (AG Turbo) for sponsoring the experimental research work. The AG Turbo is funded by German Gas Turbine Industry Companies and the Ministery of Research and Technology (BMFT).

REFERENCES

Abell, S., Hudson, J.L., 1975, "An Experimental Study of Centrifugally Driven Free Convection in a Rectangular Cavity", Int. J. Heat Mass Transfer, Vol.18, pp. 1415-1423

Arkad'ev, B.A., 1965, "A Note on Free Convection in Turbine Cavities", Journal of Engineering Physics, Vol.9, No.1

Bohn, D., Dibelius, G.H., Deuker,E., Emunds,R., 1992, "Flow Pattern and Heat Transfer in a Closed Rotating Annulus", ASME Paper, 92-GT-67

Bohn, D., Gorzelitz, V., 1992, "Experimental Investigations of Heat Transfer in a Gas-Filled Rotating Annulus", presented at the International Symposium on Heat Transfer in Turbomachinery, Athens, Greece (to be published by Hemisphere Publishing Corporation, New York)

Chew, J.W., 1985, "Computation of Convective Laminar Flow in Rotating Cavities", J. Fluid Mech., Vol.153, pp. 339-360

Farthing, P.R., Long, C.A., Owen, J.M., Pincombe, J.R., 1992, "Rotating Cavity with Axial Throughflow of Cooling Air: Heat Transfer", ASME Journal of Turbomachinery, Vol. 114, pp. 229-236

Harada, I., Ozaki, N., 1975, "A Numerical Study of the Thermal Spin-up of a Stratified Fluid in a Rapidly Rotating Cylinder", Lecture Notes in Physics, Vol.35, pp. 197-203

Hignett, P., Ibbetson, A., Killworth, P.D., 1981, "On Rotating Thermal Convection Driven by Non-Uniform Heating from Below", J. Fluid Mech., Vol.109, pp. 161-187

Kapinos, V.M., Pustovalov, V.I., Rudko, A.P., 1981, "Effect of Stabilization in Free Convetion of a Cylindrical Rotating Enclosure", Energeticeskoe masinostroenie, Nr.32, in russian, pp. 76-79

Liang, S. F., Vidal, A., Acrivos, A.; 1969, "Buoyancy-Driven Convection in Cylindrical Geometries", J. Fluid Mech., Vol. 36, part 2, pp. 239-256

Lin, T. Y., Preckshot, G.W., 1979, "Steady-State Laminar Natural Convection in a Rotating Annulus", Studies In Heat Transfer A Festschrift for E.R.G. Eckert, Hemisphere Publishing Corporation, pp. 219-246

Müller, M.R., Burch, J.N., 1985, "An Experimental Study of the Behavior of Transient Isolated Convection in a Rigidly Rotating Fluid", Experiments in Fluids, Vol.3, pp. 17-23

Ong, C.L., Owen, J.M., 1991, "Prediction of Heat Transfer in a Rotating Cavity with a Radial Outflow", ASME Journal of Turbomachinery, Vol. 113, pp. 115-122

Owen, J.M., Pincombe, J.R., Rogers, R.H., 1985, "Source-Sink Flow Inside a Rotating Cylindrical Cavity", J. Fluid Mech., Vol. 155, pp. 233-265

Patankar, S.V., Spalding, D.B., 1972, "A calculation procedure for heat, mass and momentum transfer in three-dimensional parabolic flows", Int. J. Heat Mass Transfer, Vol. 15, pp. 1787-1806

Tritton, D.J., 1988, "Physical Fluid Dynamics" (second edition), Clarendon Press, Oxford

Zysina-Molozhen, L.M., Salov, N.N., 1977, "Heat Exchange and Flow Regime of Liquids in a Closed Rotating Annular Cavity", Soviet-Aeronautics, Vol.20, No.1, pp.39-43